Angewandte Chemie
Eine Zeitschrift der Gesellschaft Deutscher Chemiker

Supporting Information

Water-Stable $DMASnBr_3$ Lead-Free Perovskite for Effective Solar-Driven Photocatalysis

Lidia Romani, Andrea Speltini, Francesco Ambrosio, Edoardo Mosconi, Antonella Profumo, Marcello Marelli, Serena Margadonna, Antonella Milella, Francesco Fracassi, Andrea Listorti, Filippo De Angelis, and Lorenzo Malavasi**

anie_202007584_sm_miscellaneous_information.pdf

SUPPORTING INFORMATION

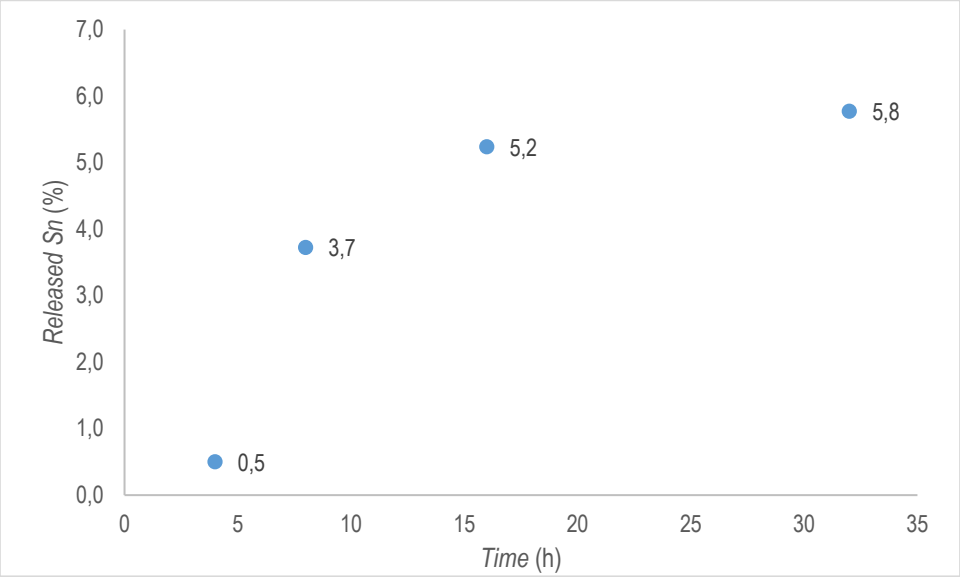

Fig. S1: Time-dependent Sn-release from $DMASnBr_3$ suspended in deionized water under stirring.

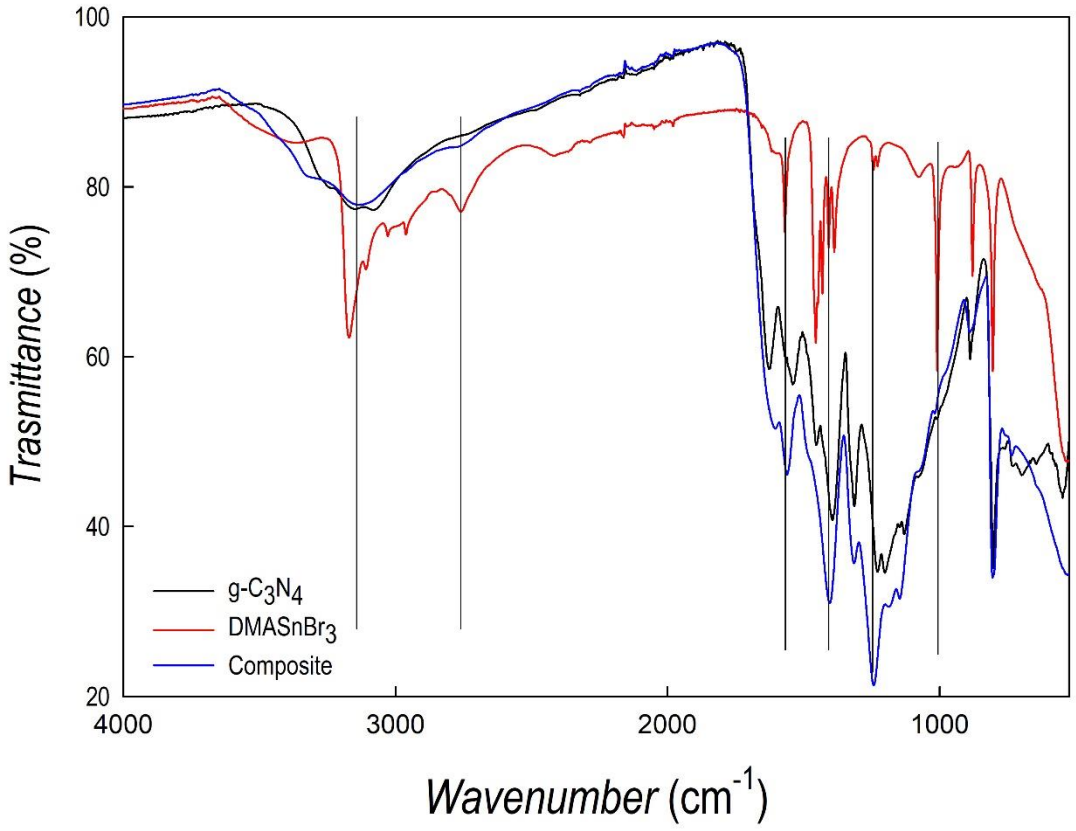

Fig. S2: FT-IR data of g-C_3N_4 (black curve), $DMASnBr_3$ (red curve) and $DMASnBr_3$@g-C_3N_4 33% (blue curve). Vertical black lines mark region of interest in the spectrum.

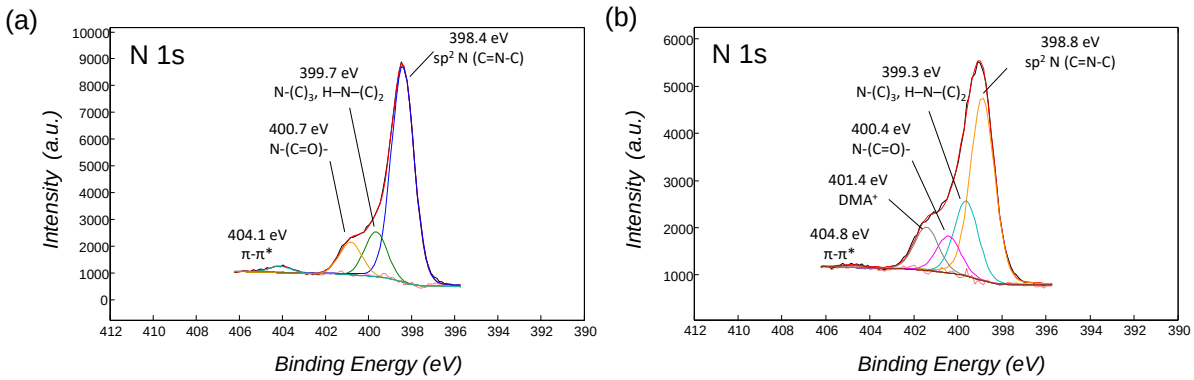

Figure S3. XPS N1s spectra of g-C_3N_4 (a) and of $DMASnBr_3$@g-C_3N_4 composite at 33wt% (b).

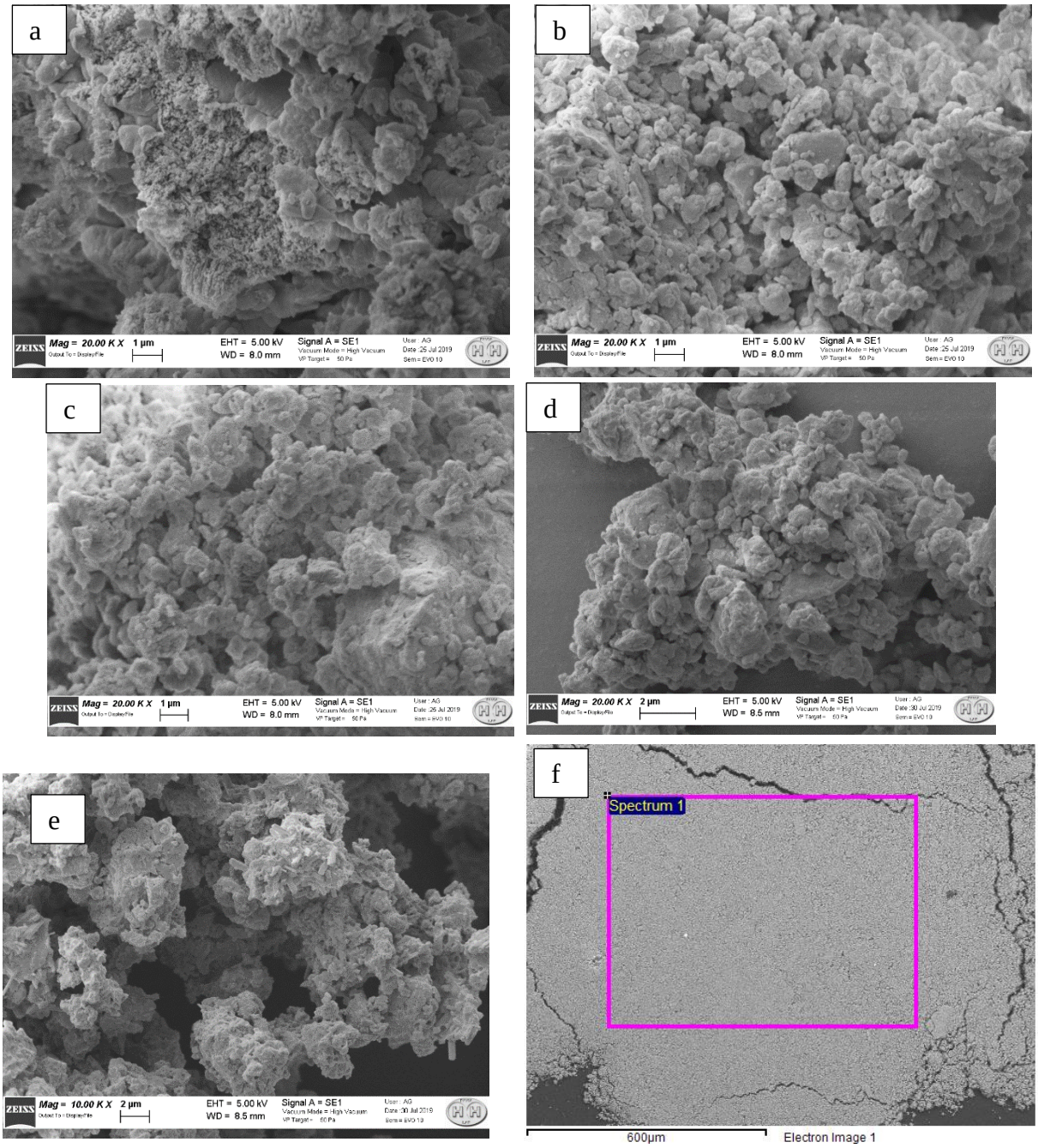

Composite (perovskite %)	exp Br/Sn (e.s.d. 5%)
33	2.89
33	3.01
33	2.91
33	2.98

Fig. S4: SEM images of a) g-C_3N_4; b) $DMASnBr_3$@g-C_3N_4 5%; c) $DMASnBr_3$@g-C_3N_4 15%; d) $DMASnBr_3$@g-C_3N_4 33%; e) $DMASnBr_3$; f) representative scan for EDX determination on $DMASnBr_3$@g-C_3N_4 33% and results of the Br/Sn ratio in the table below the figure.

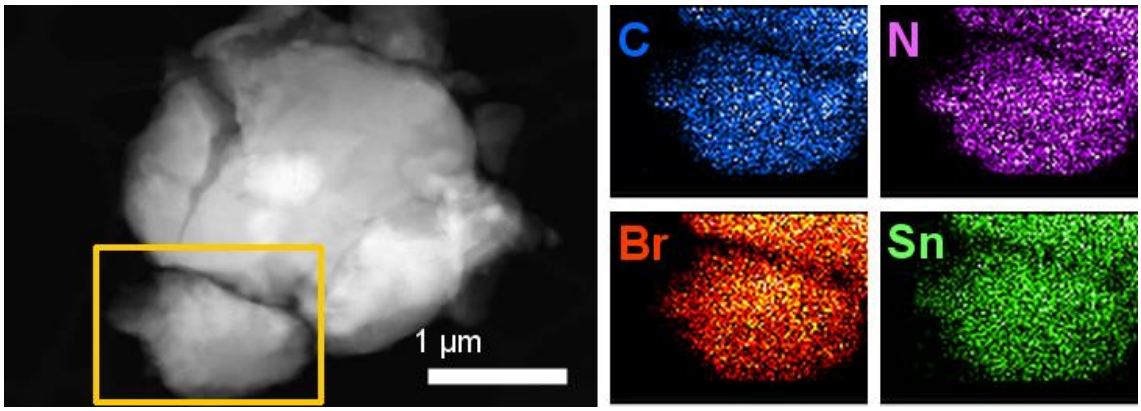

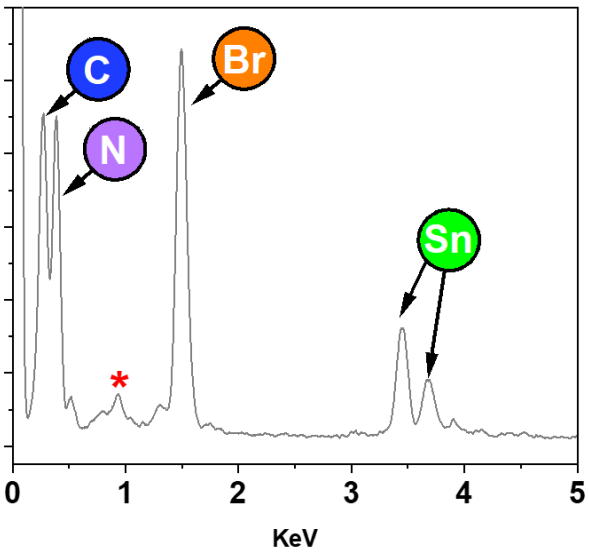

Spectrum	C	Br	Sn	Total
Sum Spectrum	25.95	45.07	28.98	100.00

All results in weight%

Figure S5: Above - STEM micrograph and related elemental distribution maps on selected area of $DMASnBr_3$@g-C_3N_4 33%; Below – EDX spectra and quantitative analysis. * peak is indexed as Cu from the Cu TEM grid.

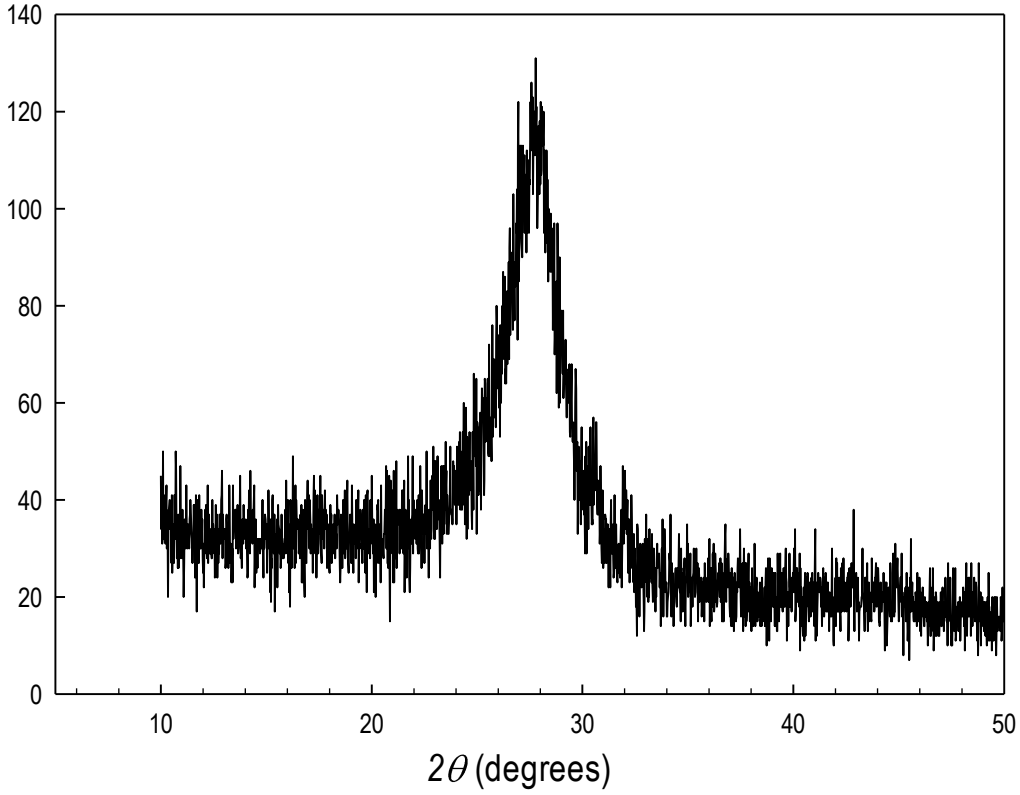

Fig. S6: XRD of the $DMASnBr_3$@g-C_3N_4 33% after photogeneration test.

Table S1. Surface area of g-C_3N_4 and $DMASnBr_3$@g-C_3N_4 composites at different percentages of metal halide perovskite loading.

Sample	Surface Area (m^2/g)
g-C_3N_4	26.4(4)
5% $DMASnBr_3$@g-C_3N_4	8.5(2)
15% $DMASnBr_3$@g-C_3N_4	5.0(4)
33% $DMASnBr_3$@g-C_3N_4	3.4(1)

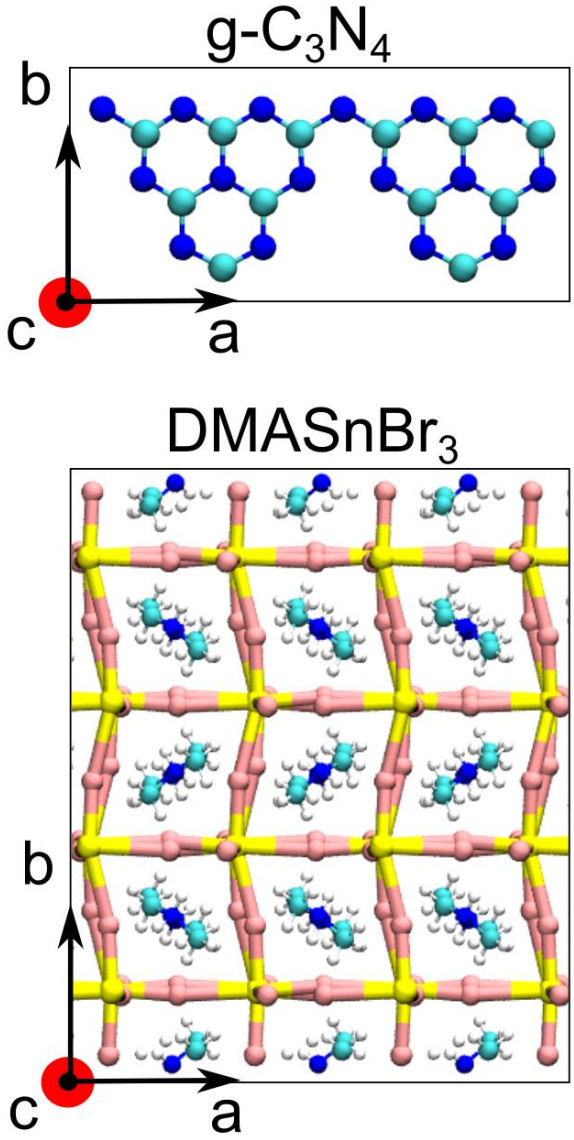

Figure S7. Ball&stick representations of the supercells used to calculate the band gap of g-C_3N_4 (top panel) and $DMASnBr_3$ (bottom panel). C in cyan, N in blue, H in white, Sn in yellow, and Br in pink.

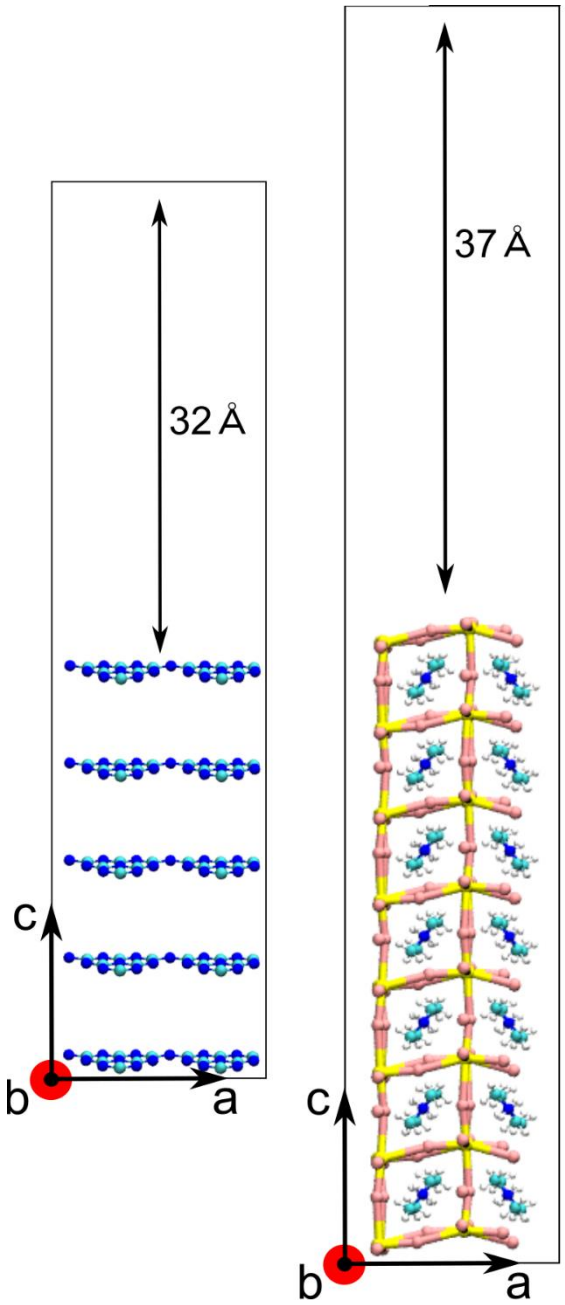

Figure S8. Ball&stick representations of the slabs employed to perform the band alignment with vacuum for g-C_3N_4 (left panel) and $DMASnBr_3$ (right panel). C in cyan, N in blue, H in white, Sn in yellow, and Br in pink.

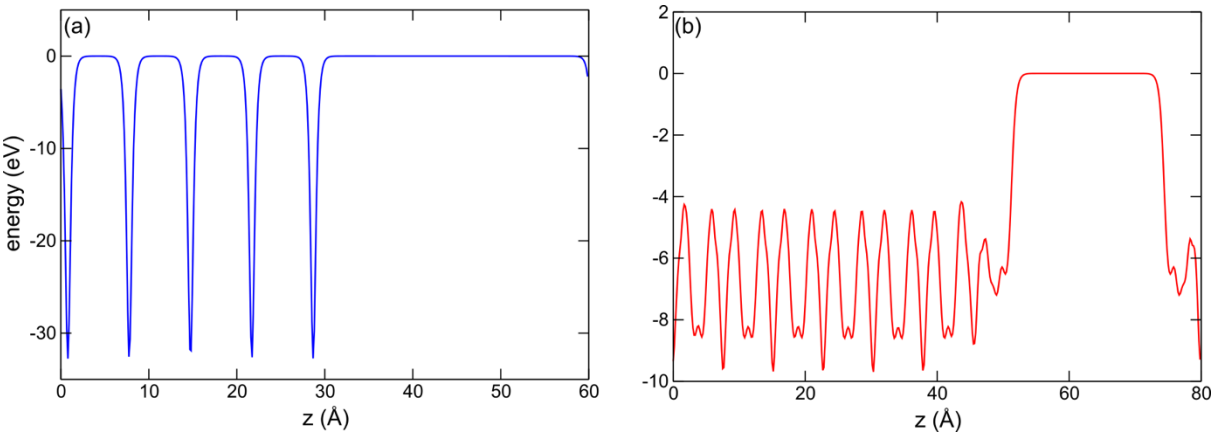

Figure S9. Average electrostatic potential across the semiconductor-vacuum interface for (a) g-C_3N_4 and (b) $DMASnBr_3$. For each system, potentials are referred to the vacuum level.

Experimental Section

Experimental Section

Bulk g-C_3N_4 has been synthesized from the polymerization of DCD ($NH_2C(=NH)NHCN$, Aldrich, 99%) by the following thermal treatment (under N_2 flux): heating (1°C/min) to 600 °C, isothermal step for 4 hours followed by cooling to room temperature (10°C/min). Synthesis has been carried out in a partially closed alumina crucible. The $DMASnBr_3$@g-C_3N_4 composite has been synthesized by ball milling. In a typical synthesis, proper amounts of DMABr, $SnBr_2$ and g-C_3N_4 have been charged under argon atmosphere in a jar and milled for 12 hours at 300 rpm (1 h cycles with 30 min stop) with a spheres/reagents ratio of 1:40.

The crystal structure of the samples has been characterized by room temperature Cu-radiation XRD acquired with a Bruker D8 diffractometer. DRS spectra were acquired in the wavelength range 300-800 nm directly on the powders by using a Jasco V-750 spectrophotometer, equipped with an integrating sphere (Jasco ISV-922). Microstructural characterization of the samples was made using a high-resolution scanning electron microscope (SEM, TESCAN Mira 3) operated at 25 kV. Surface area measures were carried out according to Brunauer, Emmett and Teller (B.E.T.) single point method by means of a Flowsorb II 2300 (Micromeritics, US) apparatus. Each sample was accurately weighed (about 0.5 g) and degassed at 80 °C for 1.5 hours under a

continuous stream of a N_2:He 30:70 mixture. Gas adsorption was then achieved by placing the sample in liquid nitrogen. Three replicates were done for each sample.

H_2 evolution experiments were conducted in distilled water containing 10% (v/v) triethanolamine (Aldrich, ≥ 99%) or 0.1 M glucose (99.9%, Carlo Erba Reagents), irradiated in Pyrex glass containers (28 mL capacity, 21 mL sample).[1] After addition of the catalyst (1 g L^{-1}), the sample was deoxygenated by Ar bubbling (20 min) to obtain anoxic conditions, and irradiated under magnetic stirring for 6 hours.

For the experiments involving use of Pt co-catalyst, Chloroplatinic acid (H_2PtCl_6, 38% Pt basis), used as precursor for metallic Pt, was from Sigma-Aldrich. Since Pt is *in situ* photodeposited on the catalyst surface, after Ar bubbling a small volume from a 15 g L^{-1} H_2PtCl_6 aqueous solution was added, using a 10-100 μL micropipette, to the catalyst suspension (1 g L^{-1}) directly in the photoreactor. The latter was closed with sleeve stopper septa and was irradiated, as described in the following, achieving simultaneous Pt deposition and H_2 production.[2] Irradiation was performed under simulated solar light (1500 W Xenon lamp, 300-800 nm) using a Solar Box 1500e (CO.FO.ME.GRA S.r.l., Milan, Italy) set at a power factor 500 W m^{-2}, and equipped with UV outdoor filter made of IR-treated soda lime glass. Triplicate photoproduction experiments were performed on all samples. The headspace evolved gas was quantified by gas chromatography coupled with thermal conductivity detection (GC-TCD), as described in previous work.[1] The results obtained in terms of H_2 evolution rate are expressed in the paper as μmoles of gas per gram of catalyst per hour (μmoles g^{-1} h^{-1}). The apparent photon flux, measured as previously reported[3], was 1.53×10^{-7} photons moles s^{-1}. The values of apparent quantum yield (AQY) were calculated as the percent ratio H_2 moles/incident photons moles[3]. XRD measurements on spent catalysts have been done by filtering the solution and recovering the powder, which underwent diffraction measurements.

XPS analyses were carried out with a Scanning XPS Microprobe (PHI 5000 Versa Probe II, Physical Electronics) equipped with a monochromatic Al K_α X-ray source (1486.6 eV), operated at 15 kV and 24.8 W, with a spot size of 100 μm. Survey (0–1200 eV) and high resolution spectra (C 1s, O 1s, N 1s, Br 3d and Sn 3d) were recorded in FAT (Fixed Analyser Transmission) mode at a pass energy of 117.40 and 29.35 eV, respectively. Surface charging was compensated using a dual beam charge neutralization system, with a flux of low energy electrons (~1 eV) combined with very low energy positive Ar^+ ions (10 eV). The hydrocarbon component of C1s spectrum was used as internal standard for charging correction and it was fixed at 284.8 eV. All spectra were collected at an angle of 45° with respect to the sample

surface. Best-fitting of the high resolution spectra was carried out with MultiPak data processing software (Physical Electronics).

Computational details

In order to align the band edges of the studied semiconductors, we employ advanced electronic-structure calculations. First, we calculate the band gap of g-C_3N_4 and $DMASnBr_3$ carrying out density functional theory (DFT) calculations at the hybrid functional level. In particular, we employ the PBE0 functional[4,5] in which the fraction of Fock exchange α is tuned, in order to reproduce the experimental gaps of these materials (2.7 eV for g-C_3N_4 and 2.85 eV $DMASnBr_3$). This functional, referred to as PBE0(α), was found to produce ionization potentials, electron affinities and energy levels at the semiconductor-water interface in remarkable agreement with the experiment.[6,7] In fact, mean average errors of ~0.2 eV have been estimated for these quantities in screenings performed on a large set of semiconductors.[5]

Hybrid-DFT calculations for bulk g-C_3N_4 and $DMASnBr_3$ are carried out with the freely-available CP2K suite of codes.[8] Goedecker-Teter-Hutter pseudopotentials are used to account for core-valence interactions.[9] We use double-ζ polarized basis sets for the wave functions[10] and a cut-off of 600 Ry for the expansion of the electron density in plane waves. We employ the auxiliary density matrix method to speed up the calculation of exact exchange in hybrid functional calculations as implemented in CP2K with the cFIT auxiliary basis set.[11] For g-C_3N_4, we employ an orthorhombic tetragonal 2×2×2 supercell with a =12.27 Å, and b = 7.08 Å, and c = 6.97 Å corresponding to the experimental density (cf. Fig. S8) . For $DMASnBr_3$, we consider a tetragonal 4×4×4 supercell with a = 24.62 Å and b = c = 24.34 Å corresponding to the experimental density (cf. Fig. S6). For both materials, a fraction of Fock exchange α = 0.18 is found to reproduce the experimental band gaps, when introduced in PBE0(α) functional. We note that our hybrid functional calculations do not include effects of spin−orbit coupling (SOC), which can be sizable for lead halide perovskites.[12,13] Therefore, we use the QUANTUM ESPRESSO code[14] and carry out hybrid functional calculations and hybrid-DFT calculations with fully relativistic optimized norm-conserving pseudopotentials.[15] In this way, we estimate the shifts induced by SOC in the position of the valence (ΔVB_{SOC}) and conduction (ΔCB_{SOC}) band of $DMASnBr_3$ and, hence, the variation of the energy gap ($\Delta E_{SOC} = \Delta VB_{SOC} + \Delta CB_{SOC}$). Our calculations give $\Delta VB_{SOC} = 0.03$ eV, $\Delta CB_{SOC} = -0.24$ eV and, $\Delta E_{SOC} = -0.21$ eV. Therefore, we fit the fraction of Fock exchange to be introduced in the PBE0(α) on the energy gap $E_g(\alpha) = E_g(\text{expt}) - \Delta E_{SOC}$, where $E_g(\text{expt})$ is the experimental band gap. Then, we

correct the position of the band edges with the respective shifts induced by SOC, in line with the procedure adopted in Ref. 6.

To align the energy levels of g-C_3N_4 and $DMASnBr_3$ with respect to the relevant redox levels of liquid water, we build surfaces of these two materials, in order to achieve interfaces with vacuum. For g-C_3N_4, we consider (i) a 5-layers 140-atoms slab with a =12.27 Å, and b = 7.08 Å, and c = 60 Å, including 30 Å of vacuum (cf. Fig. S5). The monolayer system has been also tested with negligible differences in the calculated band alignment. For $DMASnBr_3$, we employ a symmetric (100) slab with $SnBr_2$ terminated surfaces. The slab consists of 432 atoms, with a = b = 12.17 Å and c = 80 Å, the latter including 37 Å of vacuum (cf. Fig S7). For both materials, the slabs are fully relaxed with CP2K, employing the semilocal PBE functional.[16] We then determine the electrostatic-potential line-ups across the surfaces [differences below 0.03 eV in the alignment are calculated when employing the PBE0(α) functional]. In this way, the band edges of the semiconductor can be referred to the vacuum level. We note that the flat potential across the vacuum region ensures that no residual electrical field is present in the studied slabs (cf. Fig. S8). Further, we position the standard hydrogen electrode (SHE) with respect to the vacuum level. In particular, we employ the theoretical alignment presented in Ref. 17, which has been achieved combining molecular dynamics simulation of a water-vacuum interface with a computational version of the standard hydrogen electrode[17,18] (cf. Fig. 2 – main text). Finally, for the H_2O/O_2 redox level, we consider the experimental estimate placing it at 1.23 eV below the SHE.

References

[1] A. Speltini, M. Sturini, D. Dondi, E. Annovazzi, F. Maraschi, V. Caratto, A. Profumo, A. Buttafava, *Photochem. Photobiol. Sci*., **2014**, *13*, 1410-1419.

[2] L. Yang, J. Huang, L. Shi, L. Cao, Q. Yu, Y. Jie, J. Fei, H. Ouyang, J. Ye, *Appl. Catal. B,* **2017**, *204*, 335.

[3] Speltini, A.; Gualco, F.; Maraschi, F.; Sturini, M.; Dondi, D.; Malavasi, L.; Profumo, A. Photocatalytic hydrogen evolution assisted by aqueous (waste)biomass under simulated solar light: oxidized g-C_3N_4 vs. P25 titanium dioxide. *Int. J. Hydrogen Energy* **2019**, *44*, 4072-4078.

[4] Perdew, J. P.; Ernzerhof, M.; Burke, K. Rationale for Mixing Exact Exchange with Density Functional Approximations. *J. Chem. Phys*. **1996**, *105* (22), 9982−9985.

[5] Adamo, C.; Barone, V. Toward Reliable Density Functional Methods without Adjustable Parameters: The PBE0 Model. *J. Chem. Phys*. **1999**, *110* (13), 6158−6170.

[6] Guo, Z.; Ambrosio, F.; Chen, W.; Gono, P.; Pasquarello, A. Alignment of Redox Levels at Semiconductor–Water Interfaces. *Chem. Mater*. **2018**, *30*, 1 94-111.

[7] Ambrosio, F.; Wiktor, J.; Pasquarello, A. pH-Dependent Catalytic Reaction Pathway for Water Splitting at the BiVO4–Water Interface from the Band Alignment. *ACS Energy Lett*. **2018**, *3*, 829-834.

[8] VandeVondele, J.; Krack, M.; Mohamed, F.; Parrinello, M.; Chassaing, T.; Hutter, J. Quickstep: Fast and Accurate Density Functional Calculations Using a Mixed Gaussian and Plane Waves Approach. *Comput. Phys. Commun*. **2005**, *167*, 103−128.

[9] Goedecker, S.; Teter, M.; Hutter, J. Separable Dual-Space Gaussian Pseudopotentials. *Phys. Rev. B: Condens. Matter Mater. Phys*. **1996**, *54*, 1703.

[10] VandeVondele, J.; Hutter, J. Gaussian Basis Sets for Accurate Calculations on Molecular systems in gas and condensed phases. *J. Chem. Phys.* **2007**, *127*, 114105.

[11] Guidon, M.; Hutter, J.; VandeVondele, J. Auxiliary Density Matrix Methods for Hartree−Fock Exchange Calculations. J. Chem. Theory Comput. **2010**, *6*, 2348−2364.

[12] Wiktor, J.; Rothlisberger, U.; Pasquarello, A. Predictive Determination of Band Gaps of Inorganic Halide Perovskites J. Phys. Chem. Lett. **2017**, *8*, 5507-5512.

[13] Umari, P.; Mosconi, E.; De Angelis, F. Relativistic GW Calculations on $CH_3NH_3PbI_3$ and $CH_3NH_3SnI_3$ Perovskites for Solar Cell Applications. *Sci. Rep*. **2015**, *4*, 4467.

[14] Giannozzi, P.; et al. QUANTUM ESPRESSO: a Modular and Open-Source Software Project for Quantum Simulations of Materials. *J.Phys.: Condens. Matter* **2009**, *2*1, 395502.

[15] Hamann, D. R. Optimized Norm-Conserving Vanderbilt Pseudopotentials. *Phys. Rev. B: Condens. Matter Mater. Phys.* **2013**, *88*, 085117.
[16] Perdew, J. P.; Burke, K.; Ernzerhof, M. Generalized Gradient Approximation Made Simple. *Phys. Rev. Lett.* 1996, 77, 3865.
[17] Ambrosio, F.; Guo, Z.; Pasquarello, A. Absolute Energy Levels of Liquid Water. *J. Phys. Chem. Lett*. **2018**, *9*, 3212-3216.
[18] Ambrosio, F.; Miceli, G.; Pasquarello, A. Redox Levels in Aqueous Solution: Effect of van der Waals Interactions and Hybrid Functionals. *J. Chem. Phys*. **2015**, *143*, 244508.